CRYSTALLOGRAPHY REPORTS, 2025, Vol. 70, No. 1, pp. 100–106

NANOMATERIALS, CERAMICS

ELECTRICALLY CONDUCTIVE NONWOVEN MATERIALS PRODUCED BY ELECTROSPINNING OF POLYANILINE AND BULK POLYMERS

© 2025 S. N. Malakhov[a,*], Yu. N. Malakhova[a,b], and S. N. Chvalun[a]

[a] National Research Center "Kurchatov Institute", Moscow, Russia
[b] MIREA – Russian Technological University, M.V. Lomonosov Moscow State Institute of Fine Chemical Technologies, Moscow, Russia
*e-mail: s.malakhov@mail.ru

Received October 02, 2024
Revised October 14, 2024
Accepted October 14, 2024

Abstract. Electrically conductive micro- and nanofibrous nonwoven materials were obtained by electrospinning of solutions of polyaniline and a number commodity polymers (polyamide-6, polylactic acid, polystyrene, polyethylene oxide). The average fiber diameter is in the range of 0.5–6 μm, while the addition of polyaniline into the spinning solution leads to a decrease in fiber diameter. The composition of the obtained materials was confirmed by IR spectroscopy. It was found that during the electrospinning process the supramolecular structure of polyamide-6 and polylactide changes (from α-phase to γ- and amorphous phases, respectively), and polyaniline does not form crystalline structures. The specific electrical conductivity of the obtained nonwoven fabrics can reach 10^{-3} S/cm, which allows their application both in tissue engineering and in organic electronics.

DOI: 10.31857/S00234761250114e7

INTRODUCTION

Nonwoven materials possess unique physicochemical characteristics that ensure a wide range of applications in both research and commercial fields. The production of such materials by electrospinning (drawing fibers from a polymer solution or melt under the influence of a strong electric field) is currently relevant in energy generation and storage, water purification and environmental remediation, healthcare, and biomedicine [1]. At the same time, "traditional" high-volume thermoplastics and thermosets are dielectrics, as are nonwoven fabrics based on them. However, in some cases (e.g., in the field of organic electronics), these fibers need to be electrically conductive [2].

Conductive fibrous materials can be obtained by various methods. One approach is the creation of composite fibers containing a conductive filler. Such fillers may include carbon black [3, 4], carbon nanotubes [5–7], graphene and its derivatives [8–10], metals and their oxides [10–13], etc. Another approach involves coating fibers with a layer of metals or alloys, which also imparts electrical conductivity. Both steel and aluminum, as well as noble metals such as gold, silver, or platinum, can be used for this purpose [14, 15]. Finally, inherently conductive polymers can also be utilized [16].

To date, several conductive polymers are known [17], with polyaniline being one of the most convenient in terms of its combined properties (conductivity, ease of production and processing, cost) [18]. However, polyaniline in its pure form does not form fibers due to the low viscosity of its solutions. Therefore, the simplest way to obtain materials based on it is electrospinning from a mixture with a fiber-forming polymer [19–21]. When selecting a fiber-forming polymer, it is important to consider the limited solubility of polyaniline and the need for its doping – e.g., with camphorsulfonic acid or *para*-toluenesulfonic acid.

The aim of this study is to obtain hybrid nonwoven conductive materials based on polyaniline and to investigate their morphology, structure, and properties depending on the fiber-forming polymer used.

METHODS AND MATERIALS

For fiber production, the following polymers were used: polystyrene (**PS**) 525M (Nizhnekamskneftekhim, Russia) with a melt flow index (**MFI**) of 10.2; polylactide (**PLA**) 4032D (Nature Works LLC, USA) with an MFI of 7.0; polyamide-6 (**PA**) Volgamid-27 (KuibyshevAzot, Russia) with a relative viscosity of 2.74; and polyethylene oxide (**PEO**) with a molecular weight of 2,000 kDa (Sigma-Aldrich, USA). The conductive component was polyaniline (**PANI**) in the emeraldine base form (Sigma-Aldrich, USA) with a molecular weight of 10 kDa, along with camphorsulfonic acid (**CSA**) (99 %, Acros Organics). Solutions were prepared in chloroform

($CHCl_3$) (chemically pure, Komponent-Reaktiv, Russia) and hexafluoroisopropanol (**HFIP**) (99 %, PiM-Invest, Russia).

Spinning solutions were prepared by mixing the required amount of fiber-forming polymer and solvent ($CHCl_3$ for PS, PLA, and PEO; HFIP for PLA and PA) on a magnetic stirrer for 24 hours. Conductive spinning solutions were prepared in two stages: first, 200 mg of PANI and 260 mg of CSA were dissolved in 10 mL of $CHCl_3$ or HFIP and stirred on a magnetic stirrer for 24 hours. The resulting solution was filtered to remove undissolved particles, after which the fiber-forming polymer was added and stirred for another 24 hours.

Solution electrospinning was carried out using a laboratory setup (Fig. 1a) based on a Spellman SL130PN30 high-voltage power supply, a Visma-Planar DS-08 syringe pump as a dosing device, and a 50 cm diameter aluminum disk as a collector for the produced material. Conductive materials were also deposited onto glass measuring cells with pre-deposited electrodes (Fig. 1b). The applied voltage was 18 kV, the interelectrode distance was 20 cm, and the solution feed rate was 3 mL/h.

Microphotographs of the nonwoven materials were obtained using a Thermo Scientific Fisher Phenom XL scanning electron microscope at an accelerating voltage of 5 kV without conductive coating deposition. Image processing and fiber diameter determination were performed using ImageJ 1.49 software. Infrared (IR) spectroscopy was conducted using a Thermo Fisher Scientific Nicolet iS5 FTIR spectrometer with an iD5 ATR accessory for attenuated total reflection. Spectra were recorded in the 4000–550 cm^{-1} range. X-ray diffraction (XRD) analysis of the samples was performed in transmission mode using a Rigaku SmartLab diffractometer (CuK_α radiation, $\lambda = 1.5408$ Å). Contact angle measurements were conducted using a KRUSS DSA30E drop shape analysis system.

The electrical conductivity of the obtained nonwoven materials was measured using a Keithley 4200-SCS semiconductor parameter analysis system at a voltage of 1 V. The specific conductivity of the final hybrid material was calculated based on the mass and geometry of the sample.

DISCUSSION OF RESULTS

To achieve high electrical conductivity in the resulting fibers, the fiber-forming polymer content must be minimized. Therefore, the first step was electrospinning from pure polymers to determine the minimum concentration required for stable fiber formation. Electrospinning of PA solutions in HFIP was carried out within a concentration range of 2–6 wt.%. When spinning from a 2 % solution, a transition process from electrospraying to electrospinning was observed, resulting in a material consisting of particles 2–3 μm in diameter, connected by fiber fragments. Increasing the polymer concentration to 4 wt.% yielded fibers with an average diameter of ~500 nm, though some

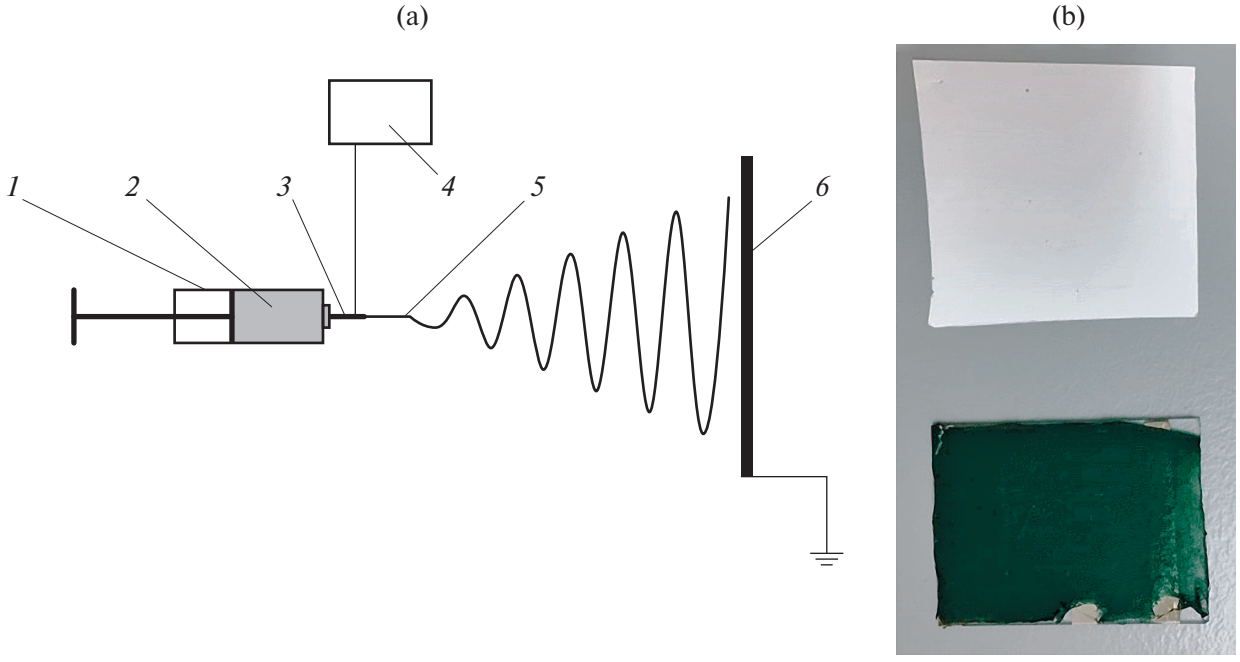

Fig. 1. Schematic diagram of the experimental setup for producing nonwoven materials (a): *1* – feeder, *2* – polymer solution, *3* – capillary, *4* – high voltage source, *5* – primary jet, *6* – receiving device. The resulting materials from pure PEO (top) and PEO–PANI/CSA, formed on a plate with applied metal electrodes (b).

spindle-shaped defects remained. Using a 6 % solution produced defect-free fibers with an average diameter of 0.7 μm. Electrospinning from a PA–PANI/CSA mixture (at a PA concentration of 6 wt.%) resulted in defect-free fibers with an average diameter of 0.6 μm (Fig. 2a).

For PLA fibers, solutions in HFIP (3–9 wt.%) and CF (4–10 wt.%) were used. Electrospinning from a 3 % PLA solution in HFIP produced fibers with numerous defects and an average diameter of 0.8 μm. Increasing the polymer content to 6 wt.% resulted in defect-free fibers with an average diameter of 1.3 μm, while at 9 wt.%, fibers reached 3.2 μm in diameter. Electrospinning from a PLA–PANI/CSA mixture (at a 6 % fiber-forming polymer concentration) reduced the average fiber diameter to 0.45 μm. Electrospinning of PLA solutions in CF at 4 wt.% led to electrospraying, while at 6 %, fibers formed but contained numerous spindle-shaped defects. At 8 %, round, defect-free fibers with an average diameter of 7.5 μm were obtained. However, adding PANI/CSA to an 8 % PLA solution caused a transition to electrospraying, resulting only in fragmented fiber segments, necessitating an increase in PLA concentration to 9 wt.%. From this solution, hybrid conductive nonwoven PLA–PANI/CSA mats with an average fiber diameter of less than 2 μm were obtained.

PEO electrospun from CF produced fibers with an average diameter of 1.2 μm at just 0.7 wt.% polymer content. The addition of PANI–CSA resulted in a minimal change in the average fiber diameter, reducing it to 1.1 μm (Fig. 2b).

Electrospinning of PS solutions at 5–10 wt.% resulted only in particle formation (electrospraying), with sizes reaching 50–70 μm. When using a 15 % solution, the material consisted of fibers (average diameter 3.2 μm) with numerous spindle- and dumbbell-shaped defects. Increasing the concentration to 20 wt.% resulted in defect-free ribbon-like fibers with an average width of 12 μm and a thickness of 4 μm, which is equivalent in cross-sectional area to round fibers with a diameter of 8 μm. Electrospinning from a PS–PANI/CSA mixture reduced the equivalent fiber diameter to 6 μm (Fig. 2c).

Thus, hybrid PANI-containing nonwoven materials can be obtained using any of the fiber-forming polymers employed in this study. However, due to significant differences in the polymer concentration required for fiber formation, the proportion of PANI in the materials varies significantly (lowest in PS-based material at 5.8 % and highest in PEO-based material at 35.7 %). This is also reflected in the appearance of the nonwoven mats: while all exhibit a green color characteristic of PANI in its emeraldine base form, their color intensity varies due to differences in the conductive component content. PS–PANI/CSA mats appear light green, PA– and PLA–PANI/CSA mats are bright green, while PEO–PANI/CSA mats (Fig. 1b) are dark green.

The wettability of the nonwoven materials is an important characteristic affecting their practical applications. The obtained nonwoven PLA and PS materials exhibit high hydrophobicity (contact angle > 130°), which is retained in conductive PLA–PANI/CSA and PS–PANI/CSA materials. Nonwoven PA material initially also demonstrates hydrophobic properties (contact angle ~140°), but after exposure to water and drying, it irreversibly loses them [26]. In contrast to pure PA mats, the hybrid conductive PA–PANI/CSA material exhibits water absorption from the outset, making it suitable for applications requiring good liquid wetting, such as tissue engineering.

During electrospinning, the polymer jet undergoes high-speed stretching in an electric field, which can alter the polymer's supramolecular structure. Analysis of wide-angle X-ray diffraction patterns indicates that the initial polyamide-6 predominantly contains α-form crystallites, corresponding to reflections at (200) at $2\theta = 20.4°$ and (002)/(202) at 23.9° [25, 26]. During electrospinning, a transition to the metastable γ-form occurs in the fibers (reflection at (200) at 21.3°), while in films cast from the spinning solution, the α-form is retained (Fig. 3a). A similar pattern is observed for polylactide (Fig. 3b): the initial polymer

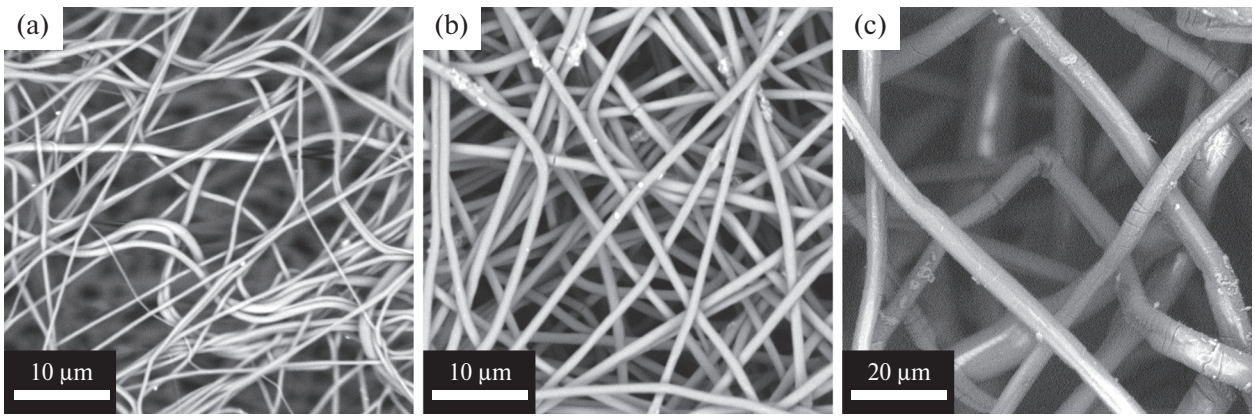

Fig. 2. Micrographs of nonwoven hybrid conductive materials based on PA (a), PEO (b) and PS (c).

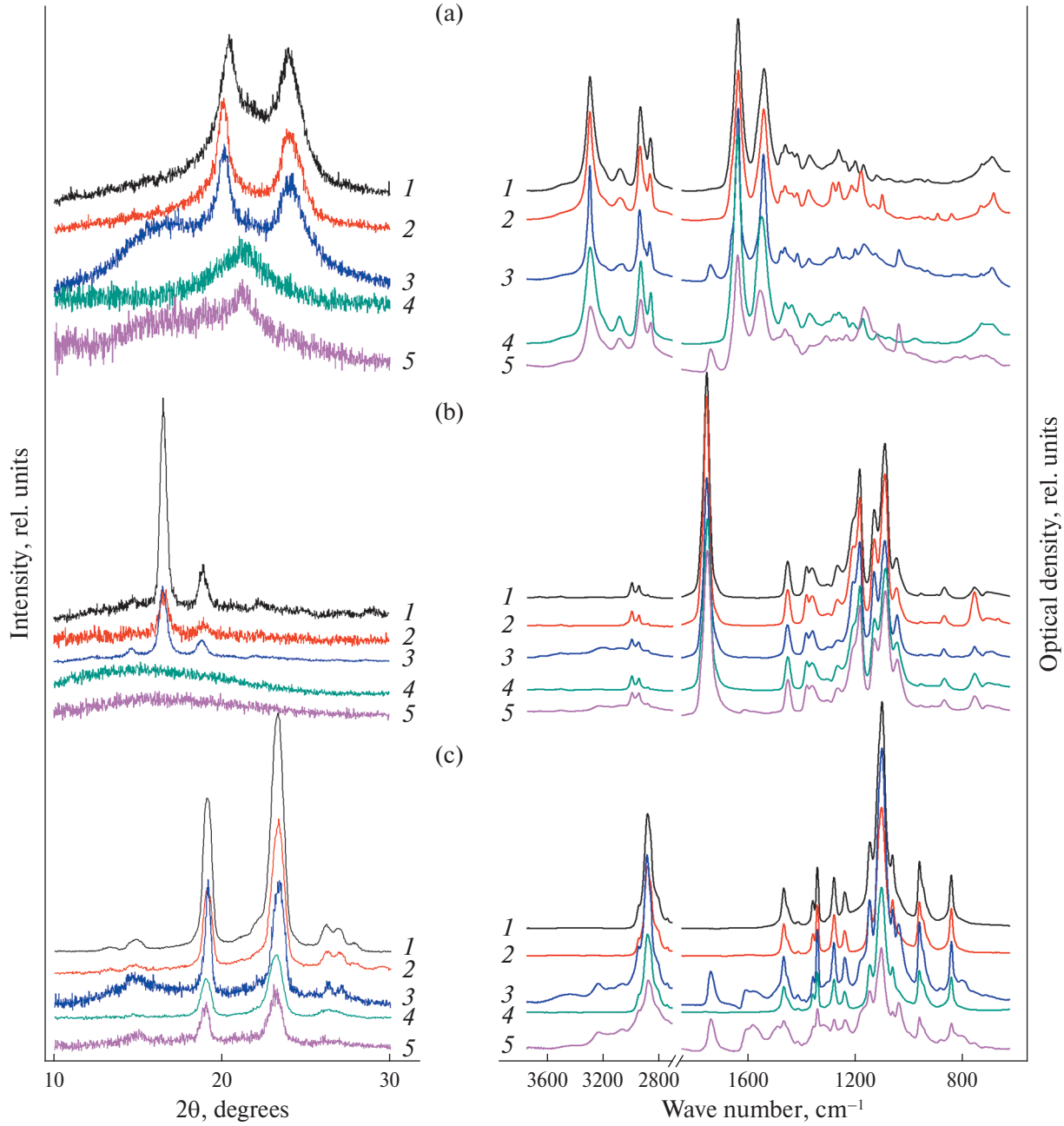

Fig. 3. Wide-angle diffraction patterns (left) and IR spectra (right) of samples based on polyamide (a), polylactide (b) and polyethylene oxide (c): *1* – initial polymer, *2* – polymer film, *3* – polymer film with PANI/CSA, *4* – non-woven polymer material, *5* – non-woven polymer material with PANI/CSA.

is partially crystalline, with reflections at (110)/(200) at 16.5° and (203) at 18.9°, characteristic of the α-phase [27, 28]. Electrospinning produces only an amorphous phase, as indicated by a broad halo in the diffraction patterns, whereas the cast films retain the original crystalline structure. In contrast, polyethylene oxide and polystyrene do not exhibit significant changes in supramolecular structure during electrospinning. For all PEO-based samples (Fig. 3c), reflections corresponding to the monoclinic crystalline phase are observed, with the most intense being (120) at 19.1° and (112) at 23.3° [29, 30]. For PS, an amorphous polymer, the diffraction patterns show only a broad halo centered at 19.4° [31, 32].

Various models of the crystalline structure of PANI/CSA are known, based on the analysis of diffraction patterns of materials with different degrees of macromolecular ordering [33]. One such model is the triclinic structure composed of double layers of PANI chains separated by double layers of CSA anions [34].

The crystallinity of solution-cast PANI/CSA films is significantly influenced by the solvent system used [35]. In particular, for HFIP and CF, a decrease in the intensity of the peak associated with intermolecular π–π interactions has been observed.

Although CSA-doped PANI can form crystalline structures, the corresponding reflections are not observed in the obtained samples (Fig. 3, curves 3 and 5). It is likely that the use of PANI/CSA mixtures with fiber-forming polymers disrupts the formation of ordered crystalline regions during electrospinning. A similar situation was described in [36] for samples based on a mixture of doped PANI with PEO, where only reflections of the fiber-forming polymer were detected. In [37], for PLA mixtures with PANI doped with p-toluenesulfonic acid, diffraction patterns of film samples exhibited a weak broad reflection in the range of 8.4°–9.5° and very weak reflections at 27.2°, 29°, and 31.4°, attributed to the doped PANI, which were not observed in the corresponding nonwoven materials. Thus, the absence of PANI/CSA reflections in nonwoven materials may be explained by a significant contribution of the amorphous phase and the high disorder of PANI chain structures [38].

The IR spectra of all samples contain absorption bands characteristic of fiber-forming polymers. For PA (Fig. 4a), these include N–H stretching vibrations (3297 cm^{-1}), Amide I (1638 cm^{-1}) and Amide II (1541 cm^{-1}) bands, C–H stretching (2934 and 2822 cm^{-1}) and bending (1463 and 1170 cm^{-1}) vibrations [25, 26]; for PLA (Fig. 4b), characteristic bands include carbonyl stretching (1756 cm^{-1}), C–O stretching (1200–1000 cm^{-1}), and C–H stretching (2995 and 2945 cm^{-1}) and bending (1454, 1383, and 1361 cm^{-1}) vibrations [24, 28]. PS is characterized by C–H stretching vibrations in the aromatic ring (3100–3000 cm^{-1}) and in methylene groups (2923 and 2850 cm^{-1}), aromatic ring vibrations (1601 and 1493 cm^{-1}), C–H bending vibrations in methylene groups (1452 cm^{-1}), and out-of-plane C–H bending vibrations in monosubstituted aromatic rings (757 and 698 cm^{-1}) [31, 32]. The IR spectra of PEO (Fig. 4c) show C–H stretching (2946 and 2884 cm^{-1}) and bending (1467, 1360, 1342, 1280, 1241, 962, and 843 cm^{-1}) vibrations, as well as C–O and C–C stretching vibrations (1147, 1100, and 1061 cm^{-1}) [23, 30].

Additionally, the spectra of conductive materials obtained from PANI/CSA mixtures contain extra absorption bands characteristic of CSA-doped PANI: N–H stretching at 3235 cm^{-1}, C–H stretching in the aromatic ring at 3070–3060 cm^{-1}, quinonoid and benzenoid ring bending vibrations at 1582 and 1491 cm^{-1}, C=N stretching at 1378 and 1304 cm^{-1}, carbonyl stretching at 1740 cm^{-1}, and sulfonyl group stretching at 1040 cm^{-1} [22–24]. Some of these bands may overlap with more intense bands of the respective fiber-forming polymer.

It should be noted that in materials obtained by electrospinning solutions, residual solvent retention is possible even after prolonged air exposure. Fig. 4 presents IR spectra fragments of PLA-based samples (films and fibers) obtained from HFIP and CF. The presence of CF is confirmed by the absorption band at 669 cm^{-1} and a significant increase in intensity at 755 cm^{-1} (where PLA and CF absorption bands overlap) [39], while the presence of HFIP is indicated by absorption bands at 894, 839, 736, and 686 cm^{-1} [40]. Therefore, when using such fibrous materials for biological and medical applications, an additional solvent removal stage is necessary to reduce their cytotoxicity.

The results of electrical conductivity measurements of the obtained materials, as well as the PANI content in the corresponding fibers, are shown in Fig. 5. As

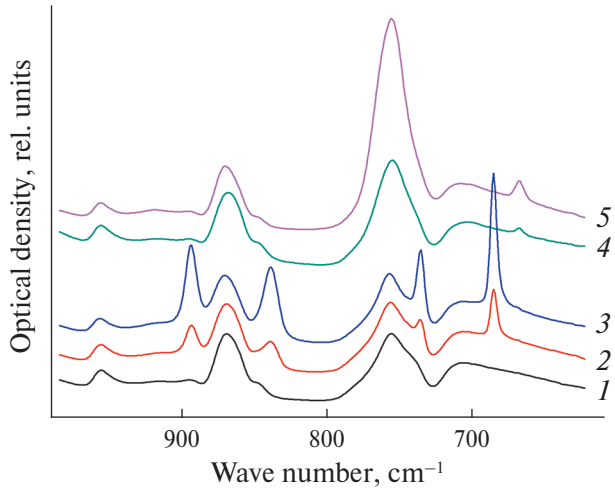

Fig. 4. IR spectra of polylactide-based samples in the range of 1000–600 cm^{-1}: 1 – initial polymer; 2, 3 – nonwoven material and film obtained from a solution in CF; 4, 5 – nonwoven material and film obtained from a solution in HFIP.

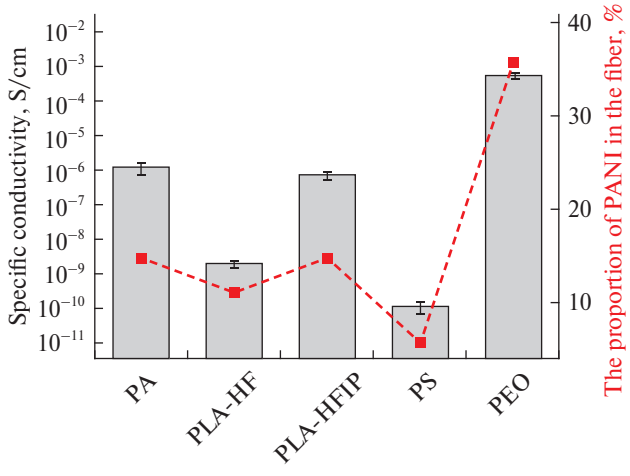

Fig. 5. Specific electrical conductivity of the obtained materials and the proportion of PANI in the fiber depending on the fiber-forming polymer used.

seen from the results, the conductivity of the samples increases with the PANI content in the fiber. The PS–PANI/CSA materials exhibit both the lowest content of the conductive component (5.8 wt.%) and the lowest conductivity (~10^{-10} S/cm). PA–PANI/CSA and PLA–PANI/CSA samples (obtained from HFIP, where fiber formation is possible at lower PLA concentrations) demonstrate conductivity of ~10^{-6} S/cm, making them suitable as matrices for electrically stimulated cell culture growth [24]. The highest conductivity (up to ~10^{-3} S/cm) is observed in nonwoven PEO–PANI/CSA fabrics, where the conductive component content is maximal (35.7 wt.%). Materials with this level of conductivity can already be used in organic electronics, such as sensors [23].

CONCLUSION

Nonwoven materials based on polyaniline and several large-scale fiber-forming polymers were obtained and characterized. The possibility of producing conductive nonwoven materials with an average fiber diameter of 0.5–6 μm was demonstrated. The addition of PANI/CSA to the spinning solution leads to a decrease in the average fiber diameter compared to the fiber-forming polymer solution, which may be related to a reduction in viscosity upon PANI introduction. During electrospinning, supramolecular structural changes occur in polyamide-6 (transition from the α- to the γ-phase) and polylactide (transition from the α- to the amorphous phase), while PANI itself does not form crystalline structures. The conductivity of the obtained materials increases with the PANI content in the fiber and can reach 10^{-3} S/cm, making them applicable in both tissue engineering and organic electronics.

FUNDING

This work was carried out as part of the state assignment of the NRC "Kurchatov Institute" using the equipment of the resource centers (OMS, EFM) of the NRC "Kurchatov Institute".

CONFLICT OF INTERESTS

The authors of this work declare that they have no conflicts of interest.

REFERENCES

1. *Kenry, Lim C.T.* // Prog. Polym. Sci. 2017. V. 70. P. 1. https://doi.org/10.1016/j.progpolymsci.2017.03.002
2. *Wang X.X., Yu G.F., Zhang J. et al.* // Prog. Mater. Sci. 2021. V. 115. P. 100704. https://doi.org/10.1016/j.pmatsci.2020.100704
3. *Hwang J., Muth J., Ghosh T.* // J. Appl. Polym. Sci. 2007. V. 104. P. 2410. https://doi.org/10.1002/app.25914
4. *Victor F.S., Kugarajah V., Bangaru M., Dharmalingam S.* // J. Electrostat. 2022. V. 119. P. 103738. https://doi.org/10.1016/j.elstat.2022.103738
5. *Mazinani S., Ajji A., Dubois C.* // J. Polym. Sci. B. Polym. Phys. 2010. V. 48. P. 2052. https://doi.org/10.1002/polb.22085
6. *Yang T., Wu D., Lu L. et al.* // Polym. Compos. 2011. V. 32. P. 1280. https://doi.org/10.1002/pc.21149
7. *Naeem F., Prestayko R., Saem S. et al.* // Nanotechnology. 2015. V. 26. P. 395301. https://doi.org/10.1088/0957-4484/26/39/395301
8. *Bao Q., Zhang H., Yang J.X. et al.* // Adv. Funct. Mater. 2010. V. 20. P. 782. https://doi.org/10.1002/adfm.200901658
9. *Azarniya A., Eslahi N., Mahmoudi N., Simchi A.* // Compos. A. Appl. Sci. Manuf. 2016. V. 85. P. 113. https://doi.org/10.1016/j.compositesa.2016.03.011
10. *Li Y., Zhang P., Ouyang Z. et al.* // Adv. Funct. Mater. 2016. V. 26. P. 2122. https://doi.org/10.1002/adfm.201504533
11. *Liu Y., Teng H., Hou H., You T.* // Biosens. Bioelectron. 2009. V. 24. P. 3329. https://doi.org/10.1016/j.bios.2009.04.032
12. *Zhu H., Du M., Zhang M. et al.* // Sensor. Actuat. B. Chem. 2013. V. 185. P. 608. https://doi.org/10.1016/j.snb.2013.05.062
13. *Alegre C., Busacca C., Di Blasi A. et al.* // J. Energy Storage. 2019. V. 23. P. 269. https://doi.org/10.1016/j.est.2019.04.001
14. *Jur J.S., Sweet III W.J., Oldham C.J., Parsons G.N.* // Adv. Funct. Mater. 2011. V. 21. P. 1993. https://doi.org/10.1002/adfm.201001756
15. *Klimova S.A., Atkin V.S., Usachev A.N. et al.* // Fibre Chem. 2017. V. 49. P. 200. https://doi.org/10.1007/s10692-017-9869-8
16. *Das T.K., Prusty S.* // Polym.-Plast. Technol. 2012. V. 51. P. 1487. https://doi.org/10.1080/03602559.2012.710697
17. *Namsheer K., Rout C.S.* // RSC Adv. 2021. V. 11. P. 5659. https://doi.org/10.1039/D0RA07800J
18. *Majeed A.H., Mohammed L.A., Hammoodi O.G. et al.* // Int. J. Polym. Sci. 2022. V. 2022. P. 9047554. https://doi.org/10.1155/2022/9047554
19. *Zhang Y., Rutledge G.C.* // Macromolecules. 2012. V. 45. P. 4238. https://doi.org/10.1021/ma3005982
20. *Das S., Sharma M., Saharia D. et al.* // Biomed. Mater. 2017. V. 12. P. 045025. https://doi.org/10.1088/1748-605X/aa7802
21. *Farkhondehnia H., Amani Tehran M., Zamani F.* // Fiber. Polym. 2018. V. 19. P. 1813. https://doi.org/10.1007/s12221-018-8265-1
22. *Frontera P., Busacca C., Trocino S. et al.* // J. Nanosci. Nanotechnol. 2013. V. 13. P. 4744. https://doi.org/10.1166/jnn.2013.7196

23. *Li C., Chartuprayoon N., Bosze W. et al.* // Electroanal. 2014. V. 26. P. 711. https://doi.org/10.1002/elan.201300641
24. *Yao J., Chen Y., Li W. et al.* // RSC Adv. 2019. V. 9. P. 5610. https://doi.org/10.1039/C8RA10495F
25. *Liu Y., Cui L., Guan F. et al.* // Macromolecules. 2007. V. 40. P. 6283. https://doi.org/10.1021/ma070039p
26. *Malakhov S.N., Chvalun S.N.* // Nanotechnol. Russ. 2020. V. 15. P. 451. https://doi.org/10.1134/S1995078020040096
27. *Hsieh Y.T., Nozaki S., Kido M. et al.* // Polym. J. 2020. V. 52. P. 755. https://doi.org/10.1038/s41428-020-0343-8
28. *Malakhov S.N., Malyshkina A.V., Chvalun S.N.* // Russ. J. Appl. Chem. 2022. V. 95. P. 1373. https://doi.org/10.1134/S1070427222090129
29. *Deitzel J.M., Kleinmeyer J.D., Hirvonen J.K., Tan N.B.* // Polymer. 2001. V. 42. P. 8163. https://doi.org/10.1016/S0032-3861(01)00336-6
30. *Malakhova Yu.N., Malakhov S.N., Kamyshinskii R.A. et al.* // Russ. J. Appl. Chem. 2017. V. 90. P. 1540. https://doi.org/10.1134/S1070427217090257
31. *Chae D.W., Kim B.C.* // Polym. Adv. Technol. 2005. V. 16. P. 846. https://doi.org/10.1002/pat.673
32. *Malakhov S.N., Kuznetsov N.M., Vdovichenko A.Y. et al.* // Fibre Chemistry. 2024. V. 55. P. 391. https://doi.org/10.1007/s10692-024-10498-y
33. *Al-Gharram M., Jum'h I., Telfah A., Al-Hussein M.* // Colloid. Surf. A. 2021. V. 628. P. 127342. https://doi.org/10.1016/j.colsurfa.2021.127342
34. *Śniechowski M., Borek R., Piwowarczyk K., Łużny W.* // Macromol. Theor. Simul. 2015. V. 24. P. 284. https://doi.org/10.1002/mats.201400105
35. *Garrudo F.F.F., Ferreira L.V., Ferraria A.M. et al.* // Synthetic Met. 2024. V. 301. P. 117523. https://doi.org/10.1016/j.synthmet.2023.117523
36. *Olvera-Gracia M., Aguilar-Hernandez J.R.* // J. Appl. Res. Technol. 2014. V. 12 P. 598. https://doi.org/10.1016/S1665-6423(14)71638-4
37. *Picciani P.H., Medeiros E.S., Pan Z. et al.* // J. Appl. Polym. Sci. 2009. V. 112. No. 2. P. 744. https://doi.org/10.1002/app.29447
38. *Ucar N., Kizildag N., Onen A. et al.* // Fiber. Polym. 2015. V. 16. P. 2223. https://doi.org/10.1007/s12221-015-5426-3
39. *Kostina Y.V., Bondarenko G.N., Alent'ev, A.Y., Yampol'skii Y.P.* // Polym. Sci. Ser. A. 2006. V. 48. P. 32. https://doi.org/10.1134/S0965545X06010056
40. *Moseti K.O., Yoshioka T., Kameda T., Nakazawa Y.* // Molecules. 2019. V. 24. P. 3945. https://doi.org/10.3390/molecules24213945